MRS Advances © 2017 Materials Research Society
DOI: 10.1557/adv.2017.247

ZnO-CuO core-shell heterostructure for improving the efficiency of ZnO-based dye-sensitized solar cells

Kichang Jung[1,3], Taehoon Lim[2,3], Yaqiong Li[3], Alfredo A. Martinez-Morales[2,3]
[1]Department of Chemical and Environmental Engineering, University of California, Riverside, California 92507, U.S.A
[2]Materials Science and Engineering Program, University of California, Riverside, California, 92507, U.S.A
[3]Southern California Research Initiative for Solar Energy, University of California, Riverside, California 92507, U.S.A

ABSTRACT

In this work, the integration of ZnO-CuO core-shell nanostructures shows improvement in the conversion efficiency of ZnO-based dye-sensitized solar cells (DSSCs). This is due to CuO acting as a secondary absorption layer that allows the absorption of near-infrared (NIR) light increasing the generated photocurrent in the device, and as a blocking layer that reduces electron-hole recombination. The ZnO core and encapsulating CuO shell are synthesized through chemical vapor deposition (CVD), and thermal oxidation of a Cu seed layer, respectively. The crystallinity of the synthesized ZnO and CuO is analyzed by X-ray diffraction (XRD). Scanning electron microscope (SEM) images show the change in morphology through the steps of Cu seed layer deposition and thermal oxidation of this layer. To determine optical properties of CuO on ZnO nanorods, UV-Vis-NIR photospectrocopy is used. The comparison of conversion efficiency of DSSCs using two different photoelectrodes (i.e. ZnO nanorods versus ZnO-CuO core-shell nanostructure) is performed by *I-V* measurements.

INTRODUCTION

Photovoltaic (PV) devices are a viable technology for helping meet future energy demands, by generating electricity from the sun—a clean, renewable, and endless source of energy [1,2]. Among the various type of the photovoltaic devices, organic-inorganic solar cells are one of the most promising technologies. Si-based solar cell panels are presently widely used due to their high efficiency, cost effectiveness, and durability. Nevertheless, new technologies such as organic-inorganic solar cells are necessary to achieve wider applications of PV devices such as in cellphones, automobiles, and wearable devices [3].

Traditionally, DSSC devices have used ruthenium-based dyes as a light absorption material. This dye can absorb ultraviolet and visible light (< 800 nm) and produce excited electrons from photon energy [4]. However, the main limitation arising from utilizing a ruthenium-based dye as an absorber is that it does not absorb infrared (IR) light (> 800nm), which accounts for 46% of sunlight [2]. This limitation of DSSCs restricts their conversion efficiency. Therefore, being able to utilize IR light has been identified as a major opportunity for improving the conversion efficiency of DSSCs [5]. Moreover, metal-oxide semiconductor materials are used as a photoelectrode in organic-inorganic solar cells. Especially for DSSCs, a semiconductor material is necessary for the transport of excited electrons from the dye to a transparent conductive substrate such as fluorine-doped tin oxide (FTO). Among metal-oxide semiconductor materials, ZnO is one of the most commonly used photoelectrode materials, due to its high electron mobility and low recombination rate. However, ZnO shows low absorption in the IR wavelength range due to its wide bandgap energy (3.37 eV) [6,7]. Alternatively, CuO is a well-known metal-oxide semiconductor material with a narrow band gap energy (1.2 eV) [8]. Therefore, CuO can be adapted as a secondary material to utilize

NIR light in DSSCs. Additionally, CuO can also help mitigate another major issue that impacts the conversion efficiency in DSSCs—the electron-hole recombination that takes place when the electrons at conduction band (CB) of the photoelectrode are recombined either within the dye, or in the electrolyte. Therefore, reducing the recombination rate is one important aspect to improve conversion efficiency in devices [9].

In this research, we show an improvement in the conversion efficiency of DSSCs using CuO as a secondary absorption layer for utilizing NIR light and a blocking layer for decreasing the charge recombination. The DSSCs are fabricated by using N719 commercial dye, and an iodide-based electrolyte. The photovoltaic characteristics of DSSCs using ZnO nanorods and ZnO-CuO core-shell nanostructures are compared by performing *I-V* measurements.

EXPERIMENT

ZnO nanorods used for the core backbone structure are synthesized by CVD on commercially available FTO glass. Zn powder located upstream the FTO glass in the CVD reactor is used as a precursor material for ZnO. The CVD reactor is ramped to the reaction temperature of 500 ^{o}C over 30 min. ramping time. Once the reaction temperature is reached, it is maintained for 30 min. The gas mixture flown into the CVD reactor is 4 sccm (oxygen), and 100 sccm (nitrogen), as the reaction and carrier gas, respectively. The CVD reactor is cooled down by natural convection after the synthesis reaction is complete. Post CVD synthesis, a 100 nm Cu seed layer is deposited on the ZnO nanorods by e-beam evaporation. The deposited seed layer is thermally oxidized in a tube furnace at 600 ^{o}C, under open environment conditions for 1 hr. For comparison and as a baseline, a Cu seed layer is also thermally oxidized on bare FTO glass for the purpose of identifying CuO peaks by XRD analysis.

During device fabrication, the synthesized ZnO-CuO core-shell nanostructure and ZnO nanorods are soaked into 0.5 mM di-tetrabutylammonium *cis*-bis(isothiocyanato) bis(2,2'-bipyridyl-4,4'-dicarboxylato)ruthenium(II) (N719) dye in ethanol solution for 70 hr. A platinum nanoparticle thin film is formed on another FTO glass by spin coating (to act as a catalyst). The two substrates (photoelectrode and counter electrode) are sandwiched and sealed with a surlyn film, with a 25 µm thickness. The gap between the two substrates is filled with an iodine-based electrolyte. The electrolyte solution is made of 0.05 M of LiI, 0.03 M of I_2, 0.5 M of 4-*tert*-Buthylpyridine and 0.1 M of guanidine thiocyanate mixed in the solvent with valeronitrile and acetonitrile solution in 1:1 volume ratio.

The surface morphology of the synthesized ZnO-CuO core-shell nanostructure and ZnO nanorods is analyzed using SEM (FEI Nova NanoSEM 450). The crystalline structure is investigated by XRD in a Panalytical X'Pert XRD instrument using Cu Kα radiation. The transmittance of the synthesized materials is measured by Varian Cary 500 double beam scanning UV/Vis/NIR spectrophotometer (200 nm to 1500 nm). To analyze photovoltaic properties, a Xenon lamp and a semiconductor analyzer are used.

DISCUSSION

As shown in Figure 1 (a), (b), and (c), the SEM images show different morphologies for ZnO nanorods, ZnO-Cu, and ZnO-CuO core-shell nanostructures. Figure 1 (a) shows that quasi-1D ZnO nanorods are synthesized by CVD on the FTO glass. The ZnO shape is hexagonal pillar and the surface of the tip is flat. The mean diameter of the ZnO nanorods is 47 nm. The morphology of the deposited Cu seed layer on ZnO nanorods is shown in Figure 1 (b). The surface morphology is significantly changed by the deposition of the Cu seed

layer, and shows a rougher surface. This is because Cu is deposited as a cluster of particles rather than as a smooth film during e-beam deposition.

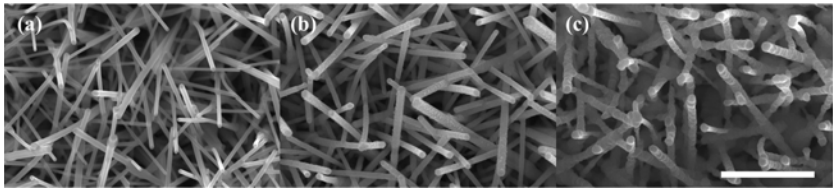

Figure 1. SEM images of the surface morphology of synthesized materials: (a) ZnO nanorods, (b) ZnO-Cu, and (c) ZnO-CuO core-shell nanostructures. The white bar indicates 1 μm scale.

In comparison to the ZnO nanorods, the ZnO-Cu core-shell nanostructures show a wider diameter (69 nm), due to the Cu layer thickness. However, the thickness of Cu seed layer is not 100 nm due to it is calculated based on the assumption that the surface is flat. The Cu particle size is 29 nm. It can be seen that the surface area increases after Cu deposition. This is because each ZnO nanorod surface area enlarges without affecting the quantity of nanorods. Figure 1(c) shows ZnO-CuO core-shell nanostructures after a thermal oxidation process. The diameter of the core-shell is increased to 85 nm. The morphology of the shell is changed into a much rougher surface due to the Cu seed layer agglomerating during the oxidization.

Figure 2 shows the XRD patterns of ZnO-Cu core-shell nanostructure, CuO layer on FTO glass, and ZnO-CuO core-shell nanostructure from 33.0º to 45.0º. Both of the core-shell nanostructures have a typical wurtzite hexagonal ZnO crystal structure with peaks located at 34.4º, 36.2º, and 37.7º, as shown by the black and blue XRD patterns. After thermal oxidation of Cu seed layer on the FTO glass, two of CuO peaks are shown at 35.5º and 38.7º. They are correlated with [-111] and [111] directional preference. The ZnO-CuO core-shell nanostructure has ZnO and CuO peak each and there is no peak shift.

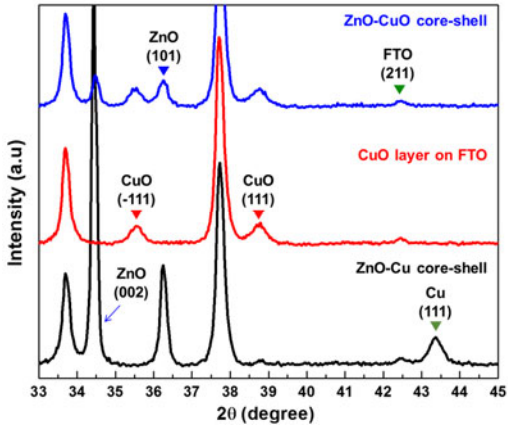

Figure 2. XRD pattern of the Cu-ZnO core-shell nanostructure (bottom), CuO layer on FTO glass (middle), and ZnO-CuO core-shell nanostructure (top).

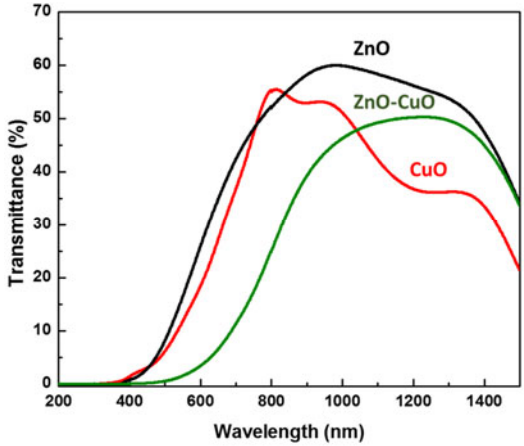

Figure 3. Optical transmittance spectrum of ZnO nanorods, CuO and CuO-ZnO core-shell nanostructure, from 200 nm to 1500 nm.

Figure 3 shows the optical transmittance for all samples measured from 200 nm to 1500 nm by UV-Vis-NIR photospectroscopy. The result shows light above 400 nm passes through ZnO nanorods due to its wide band gap (3.37 eV). Especially, high transmittance is observed in range of NIR (> 800 nm). On the other hand, the CuO layer on FTO glass shows low transmittance above 800 nm. This is due to the narrow band gap of CuO (1.2 eV). The ZnO-CuO core-shell nanostructure has lower transmittance than ZnO nanorods due to CuO shell assisting as an absorption layer on the ZnO nanorods. The performance comparison of DSSCs using ZnO nanorods and ZnO-CuO core-shell nanostructures is shown in Figure 4.

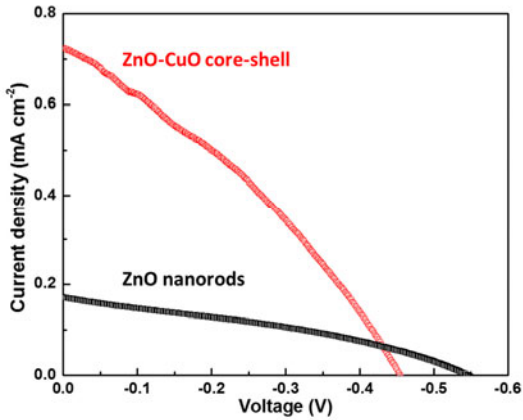

Figure 4. Photocurrent as a function of photovoltaic characteristics for DSSCs fabricated ZnO nanorods (bottom) and ZnO-CuO core-shell nanostructure (top).

Higher conversion efficiency (0.108%) is obtained by using ZnO-CuO core-shell nanostructure as a photoelectrode in DSSC compared to ZnO nanorods (0.032%). Especially, the ZnO-CuO-based device has a photocurrent density 4.2 times higher than ZnO nanorods, as shown in Table 1.

Table 1. Solar cells parameters of ZnO nanorods and ZnO-CuO core-shell nanostructures.

Photoelectrode	J_{sc} (mA/cm^2)	V_{oc} (V)	Fill Factor	Efficiency (%)
ZnO nanorods	0.17	0.545	0.347	0.032
ZnO-CuO core-shell nanostructure	0.72	0.456	0.328	0.108

The observed increased performance can be attributed to a higher photocurrent resulting from two separate mechanisms. First, the CuO shell on the ZnO core absorbs and utilizes more visible and NIR light, generating a larger number of excited electrons, as shown in Figure 3. Second, the CuO shell structure behaves as a blocking layer that reduces interfacial recombination by inhibiting electrons from moving back to the highest occupied molecular orbital (HOMO) of the dye, or electrolyte. Thus, minimizing current leakage paths and improving the photocurrent density in the device. This is because the CB of CuO shell (-0.84 eV vs. NHE) [10] is situated above the CB of ZnO (-0.25 eV, NHE) [11]. The inclusion of the CuO shell promotes charge transfer from the dye to the ZnO photoelectrode, as shown Figure 5 [12]. In particular, CuO prevents electron transfer from ZnO to the HOMO level of the dye and electrolyte, while thermodynamically allowing electron injection to the ZnO. As a result, the ZnO-CuO core-shell nanostructure increases the current density by reducing recombination of electrons and holes at the interface.

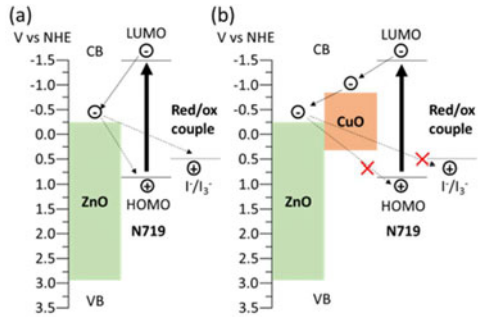

Figure 5. Energy diagram of (a) ZnO nanorods and (b) ZnO-CuO core-shell nanostructure as a photoelectrode in DSSCs.

Futhermore, the inverse of the slope at the V_{oc} (shown in Figure 4) is proportional to the series resistance of the cell. The series resistance in solar cells is affected by the movement of current from the dye, to the photoelectrode, to the FTO glass, to the metal contact. The cell using ZnO-CuO core-shell nanostructure shows an increased slope compared to the one fabricated with ZnO nanorods at the V_{oc}, indicative of a reduction in series resistance. The CuO shell on the ZnO core acts as a blocking layer that leads to a lower series resistance, reducing the recombination of electron-hole pairs, and enhancing

photocurrent generation [12,13]. In this work, we explore the effect of CuO layer on ZnO nanorods for 1) increasing the absorption range; and, 2) lowering electron-hole recombination.

CONCLUSIONS

In summary, we have successfully demonstrated improvement in the conversion efficiency in DSSCs using ZnO-CuO core-shell nanostructure in comparison to ZnO nanorods. The CuO shell is synthesized on ZnO by thermal oxidation. Further optimization is necessary to reduce the amount of defects during the CuO shell formation, and increase conversion efficiency. To further validate our results presented here, we will fabricate and characterize more devices to confirm repeatability and obtain average performance in terms of open circuit voltage, short circuit current, fill factor, and conversion efficiency. Future work will focus on decreasing recombination at the interface.

ACKNOWLEDGEMENTS

The characterization work was conducted at the Central Facility for Advanced Microscopy and Microanalysis (CFAMM) at UCR. This research was partially funded by the University of California Advanced Solar Technologies Institute (UC Solar).

REFERENCES

1. Martin I. Hoffert, Ken Caldeira, Atul K. Jain, Erik F. Haites, L. D. Danny Harveyk, Seth D. Potter, Michael E. Schlesinger, Stephen H. Schneider, Robert G. Watts, Tom M. L. Wigley, and Donald J. Wuebbles, *Nature*, **395**, 881-884 (1998)
2. J. Blanco, S. Malato, P. Fernández-Ibañez, D. Alarcón, W. Gernjak, and M.I. Maldonado, *Renew. Sust. Energ. Rev.*, **13**, 1437-1445 (2009)
3. Matthew Wrigh, and Ashraf Uddin, *Sol. Energ. Mat. Sol. C.*, **107**, 87-111 (2012)
4. Shufang Zhang, Xudong Yang, Youhei Numata, and Liyuan Han, *Energy Environ. Sci.*, **6**, 1443-1464 (2013)
5. Liyaun Han, Ashraful Islam, Han Chen, Chandrasekharam Malapaka, Barreddi Chiranjeevi, Shufang Zhang, Xudong Yang, and Masatoshi Yanagida, *Energy Environ, Sci.*, **5**, 6057-6060 (2012)
6. Oana Carp, AlinaTirsoaga, Bogdan Jurca, Ramona Ene, Simona Somacescu, and Adelina Ianculescu, *Carbohyd. Polym.*, **115**, 285-293 (2015)
7. H. Cao, J. Y. Xu, D. Z. Zhang, S.-H. Chang, S. T. Ho, E. W. Seelig, X. Liu, and R. P. H. Chang, *Phys. Rev. Lett.*, **84**, 5584-5587 (2000)
8. Dangxin Wu, Qiming Zhang and Meng Tao, *Phys. Rev. B*, **73**, 235206 (2006)
9. Michael Grä1tzel, *Inorg. Chem.*, **44**, 6841-6851 (2005)
10. Michael Woodhouse and B. A. Parkinson, *Chem. Soc. Rev.*, **38**, 197-210 (2009)
11. Samantha S. Wilson, Jeffrey P. Bosco, Yulia Tolstova, David O. Scanlon, Graeme W. Watson and Harry A. Atwater, *Energy Environ. Sci.*, **7**, 3606-3610 (2014)
12. Phathaitep Raksa, Sanpet Nilphai, Atcharawon Gardchareon, Supab Choopun, *Thin Solid Films*, **517**, 4741-4744 (2009)
13. R. Sahay, J.Sundaramurthy, P.SureshKumar, V.Thavasi, S.G.Mhaisalkar, S.Ramakrishna, *J. Solid State Chem.*, **186**, 261-267 (2012)